C. R. Mecanique 347 (2019) 19–32

Contents lists available at ScienceDirect

Comptes Rendus Mecanique

www.sciencedirect.com

A model for the aerodynamic coefficients of rock-like debris

Vincent Chai [a], Dushyant Parkhi [a], Sethu Boopathy [a], Junting Xiang [a,b,c,*], Jörg Schlüter [a,b,**]

[a] Nanyang Technological University, 50 Nanyang Avenue, 639798, Singapore
[b] Deakin University, School of Engineering, 75 Pigdons Road, VIC 3216, Australia
[c] CSIRO Manufacturing, Private Bag 10, Clayton, VIC 3168, Australia

ARTICLE INFO

Article history:
Received 18 August 2018
Accepted 5 October 2018
Available online 8 November 2018

Keywords:
Wind-tunnel test
Aerodynamic coefficients
Rock-like debris
Model prediction
Debris trajectory

ABSTRACT

This study presents a model to determine the aerodynamic forces on an irregularly shaped object for prediction of trajectories of debris. We classify the debris according to shape and use wind tunnel tests to create a database of aerodynamic forces of similarly sized objects. We have then validated the database results against wind tunnel measurements of aerodynamic coefficients of rock-like debris objects. Although the individual errors may be significant, the results show a generally good agreement with our model prediction and a small average error.

1. Introduction

The explosion of ammunition storage magazines can pose a serious threat to the surrounding area. The prediction of the range of debris flight is vital in order to avoid injuries and damage to other buildings and to derive design recommendations on the minimum distance required between buildings close to the magazine. At the initial stage of explosion, the debris is traveling at very high speed. As a result, the range of the debris flight is strongly dependent on the aerodynamic drag forces [1–3]. However, as the number of debris particles is at least tens of thousands, the computational cost to conduct a full Computational Fluid Dynamic (CFD) simulation for each debris particle is prohibitively high, though CFD has been demonstrated to be a feasible approach for many applications [4–7], including particle tracking [8,9] or particle-laden flows [10,11]. The possible approach to handle particle–particle and particle–fluid interactions together is the DEM–CFD method (DEM: discrete element method), when a limited number of particles are included [9]. However, the DEM–CFD method is usually applied for regularly shaped objects such as spheres and relatively small sized objects [12], whereas in the present study mostly irregularly shaped objects (high-aspect-ratio debris) are of our concern. Hence, a simplified model is required to estimate the aerodynamic coefficients of a given single debris object, such that the coefficients can be further utilized in the flight equations to determine the trajectory and range of each debris object. We will present here such a model. In this model, each debris object is categorized and then the aerodynamic coefficients determined from a database of wind tunnel data of similarly shaped objects are presented.

* Corresponding author at: CSIRO Manufacturing, Private Bag 10, Clayton, VIC 3168, Australia.
** Corresponding author.
E-mail addresses: jerry.xiang@csiro.au (J. Xiang), jorg.schluter@deakin.edu.au (J. Schlüter).

https://doi.org/10.1016/j.crme.2018.10.001
1631-0721/

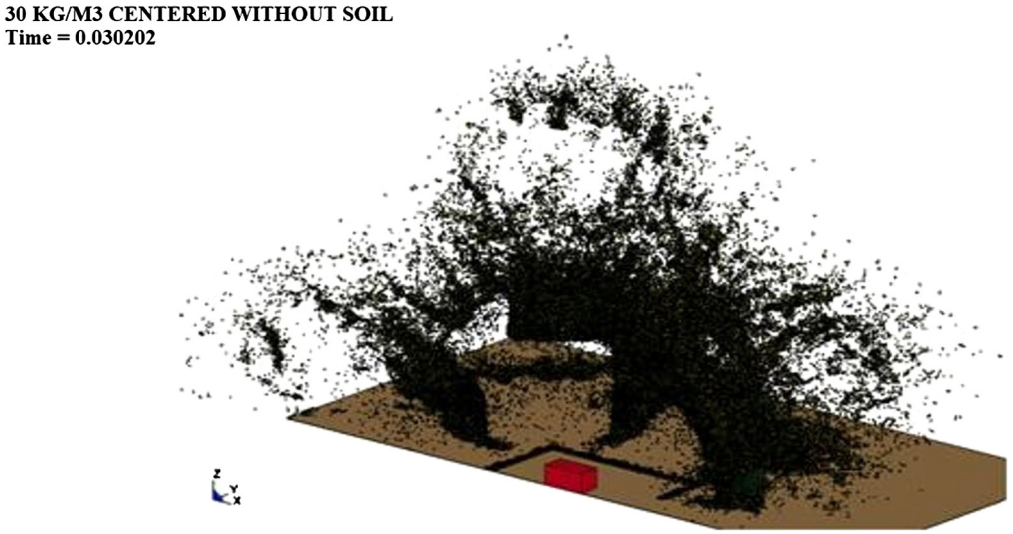

Fig. 1. Numerical simulation of the initial break-up of an ammunition storage magazine after an accidental explosion.

Model structure

1.1. Background

Ammunition storage magazines always pose a threat through accidental explosion. To minimize the damage to the surroundings, these magazines need to be located at a safe distance from populated areas. To determine the distance that can be considered safe, a design tool is required to estimate the range and energy of the debris following an explosion. The analysis of an exploding storage magazine needs to be performed in several steps:

1) determination of the initial explosion and the break-up of the structure;
2) computation of the flight trajectories of the debris particles;
3) analysis of impact and ricochet of the debris.

In this study, we concentrate on the second step: the computation of the flight trajectory. The flight trajectory is characterized by the high initial velocities at which the debris is ejected, even reaching almost the speed of sound. As mentioned, at such high speed, the range of the debris flight is strongly dependent on the aerodynamic drag forces. A previous study by Fan et al. [13] on the influence of the drag coefficient in the range of $0.0 < C_D < 2.0$ showed significant effects of the drag coefficient on the range of the trajectory.

The simulation of the initial break-up of the structure of the ammunition storage magazine provides a very large number of irregularly shaped objects (Fig. 1 [13]), ranging from tens of thousands to several million. An accurate determination of the aerodynamic forces based on the exact shape of each object by computational or experimental means is therefore not feasible. Hence, a simplified model providing an estimate of the aerodynamic characteristics is required.

1.2. Previous work

In the past two decades, researchers have been working on the simulation of the flight of debris mainly under the influence of wind. The challenges that they faced were to characterize the shape and size of the debris, the boundary conditions, and the precise aerodynamic parameters. Richards [14] stated that the dispersion of windborne debris was caused by the object's aerodynamic performance and shape. In addition, Held [15] concluded that the variation of the air drag coefficient with shape had a significant effect on the ejecting velocity of the object after explosion.

To account for the shape effects in the trajectory of debris, Wills et al. [16] studied the flight of windborne debris and classified it as compact bodies, sheets, and rods. Tachikawa [17] studied the debris trajectories in a wind tunnel, classifying the debris as small flat plates and prisms, and numerically calculated the trajectories by assuming constant aerodynamic coefficients at low speed, with consideration of the auto rotational effect of plates through measurements of drag and lift due to rotation in a wind tunnel.

In addition, numerical calculations of trajectories of plates of square plan-form were made by Holmes et al. [18], and the results were compared with experimental data. Additionally, Holmes studied the effect of horizontal and vertical velocities on the windborne debris in severe windstorms [19]. Baker [20] also identified several dimensionless parameters that significantly affected the flight of debris through analytical and numerical study of compact and sheet debris.

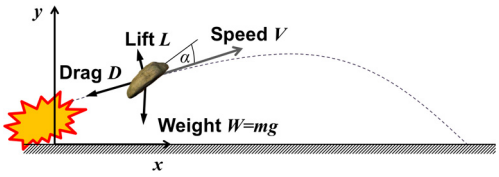

Fig. 2. Forces acting on airborne debris.

Michael Grayson et al. [21] have proposed a probabilistic model for predicting the variation of debris trajectories in three-dimensional space. In addition, Karimpour et al. [22] have concluded that underestimations of the mean flight distance and mean impact kinetic energy were possible, if the debris flight simulation failed to account for the uncertainty of the debris size, horizontal and vertical turbulence intensity.

In recent years, several debris-throw prediction models have been developed and published through the Department of Defense Explosives Safety Board (DDESB). These include:

- the TRAJ model [23], which includes the effects of projectile mass, shapes, density, launch velocity and launch angle, and multiple ricochets;
- the KG-ET model [24], which was used for the prediction of debris throw from reinforced concrete structures after an accidental explosion, assuming a cubical shape of the debris to determine the Mach-number-dependent drag coefficients;
- the UK-model [25] used a calculated launch velocity of a broken structure and a simplified point mass model, with drag-dependent mass, reference cross-sectional area, and a fixed drag coefficient C_D between 1.0 and 2.0 to compute the flight path;
- the DeThrow model from PTRC-NTU computed debris trajectory using a constant drag coefficient of 1.2.

All of these models used either a constant drag coefficient C_D or only very simple drag predictions. In most cases, the shape of the debris was assumed as a sphere or a cube, and the orientation was not taken into account. Hence, in this study, a detailed investigation of the drag coefficients is conducted to arrive at a more accurate prediction model.

1.3. Debris flight equations

The flight translation of a single fragment can be described with the equations below (in three-dimensional vector form, with three degrees of freedom):

$$m\ddot{\boldsymbol{x}}(t) = \sum \boldsymbol{f} \tag{1}$$

where m is the mass of the fragment, $\boldsymbol{x}$ is the translational position vector, and $\ddot{\boldsymbol{x}}$ is the second time derivative of the translational position vector of the fragment. The vector $\boldsymbol{f}$ is the sum of all the forces that act on the fragment, which include the gravitational force and the aerodynamic forces.

We do not consider the rotational degrees of freedom as these do not influence the trajectory directly. The rotational speed only plays a role if the rotation of the object is sufficiently large to affect the lift coefficient by the Magnus effect.

The aerodynamic forces that we consider here can be expressed as a drag force D acting in the direction of the flight path and a lift force L acting perpendicular to the flight path (Fig. 2):

$$D = \frac{1}{2}\rho V^2 \cdot C_D \cdot A \tag{2}$$

$$L = \frac{1}{2}\rho V^2 \cdot C_{L,\text{total}} \cdot A \tag{3}$$

with ρ the density of the air, V the airspeed of the debris, A the projected area facing the flow, and C_D and $C_{L,\text{total}}$ the aerodynamic coefficients. The airspeed experienced by the debris consists of the flight speed of the debris and the wind speed. Air motion affected by the cloud of debris is not considered in the present study. The lift force can then be split into the lift due the object's shape C_L and the lift due to the rotation of the object C_{LA} (Magnus effect):

$$C_{L,\text{total}} = C_L + C_{LA} \tag{4}$$

Furthermore, we consider the trajectory largely two dimensional, which means that the debris motion remains within the plane defined by the initial velocity and the acceleration direction.

Baker [20] has simplified the equation of motion of a debris particle under these conditions to:

$$m\frac{\mathrm{d}^2x}{\mathrm{d}t^2} = \frac{A\rho}{2}\left(C_D\cos\alpha - (C_L + C_{LA})\cdot\sin\alpha\right)\cdot\left((U_w - u)^2 + (V_w - v)^2\right) \tag{5}$$

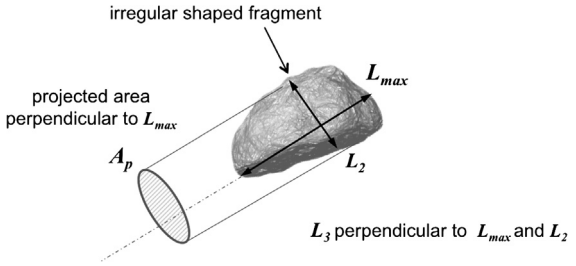

Fig. 3. Definition of the geometrical parameters of the debris.

$$m\frac{\mathrm{d}^2 y}{\mathrm{d}t^2} = \frac{A\rho}{2}\left(C_\mathrm{D}\sin\alpha + (C_\mathrm{L} + C_\mathrm{LA})\cdot\cos\alpha\right)\cdot\left((U_\mathrm{w} - u)^2 + (V_\mathrm{w} - v)^2\right) - mg \tag{6}$$

Here U_w and V_w are the components of the atmospheric wind velocity in the x and y directions, respectively. Note that A is an instantaneous value of the projected area facing the flow when rotation of object is considered. For the high speeds encountered in the explosion of ammunition storage magazines, the wind component is negligible and the equations simplify to:

$$m\frac{\mathrm{d}^2 x}{\mathrm{d}t^2} = \frac{A\rho}{2}\left(C_\mathrm{D}\cos\alpha - (C_\mathrm{L} + C_\mathrm{LA})\cdot\sin\alpha\right)\cdot\left(u^2 + v^2\right) \tag{7}$$

$$m\frac{\mathrm{d}^2 y}{\mathrm{d}t^2} = \frac{A\rho}{2}\left(C_\mathrm{D}\sin\alpha + (C_\mathrm{L} + C_\mathrm{LA})\cdot\cos\alpha\right)\cdot\left(u^2 + v^2\right) - mg \tag{8}$$

Since the mass and the initial trajectory α are given by the initial break-up simulation, suitable estimates for the aerodynamic coefficients C_L and C_D are needed for the solution to the debris flight equation.

1.4. Factors influencing aerodynamic coefficients

The aerodynamic coefficients of a debris object at high speed are influenced by a number of factors:

1) the shape of the object;
2) the Mach number of the object, where the Mach number is defined as $M = V/a$, with a being the speed of sound and V the speed of the object;
3) the proximity of the object to other debris objects ("cloud effect"), which means that some debris can decrease their drag in the slipstream of the preceding debris;
4) the rotational speed of the object (Magnus effect). This effect can be observed, e.g., in spinning table tennis balls that display a curved trajectory.

A model that estimates the aerodynamic coefficients for the explosion of ammunition storage magazines needs to consider all of these effects to be sufficiently complete. However, here, we would like to focus on the shape drag as it is considered to be the most important.

1.5. Analysis of the initial break-up debris shapes

Since the shape of the object is one of the most important factors in determining the drag, we study simulations of the initial break-up of the structure to narrow down the possible shapes that can be encountered. Berglund et al. [26] conducted break-up tests with small "ammunition houses" according to Kasun-II Test 2 [27] – Above Ground Magazine (AGM-25). Fan et al. conducted a series of numerical simulations of the initial break-up during this test [13].

From this simulation database, a classification of the shapes directly after break-up can be performed. We define the aspect ratio AR of each object as:

$$AR = \frac{L_\mathrm{max}}{\sqrt{A_\mathrm{p}}} \tag{9}$$

where L_max is the longest diameter of debris, A_p is area of the projection orthogonal to L_max (see Fig. 3). We can further determine the lengths of the object L_2 and L_3 perpendicular to L_max and perpendicular to each other, where L_2 is the second largest length and L_3 the shortest length. The shape of each object can then be further classified according to these lengths and defined as debris shape ratio of L_max: L_2: L_3.

To determine the probability of occurrence of each shape from the initial break-up, the data of Fan et al. [13] are used to classify each debris object according to its length ratios and plotted as a probability density function (Fig. 4). We can

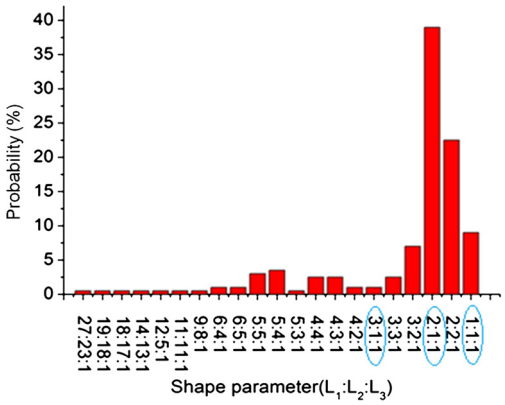

Fig. 4. Probability density function of the geometric shapes found at the initial break-up.

identify that the ratios of debris shape of 1:1:1, 2:1:1 and 2:2:1 dominate the debris cloud. Furthermore, there are a number of elongated debris (3:1:1, 4:2:1, etc.) that can be collectively described as elongated bodies.

While previous studies focused on plate-like debris, we can see that plate-like debris (e.g., aspect ratios of 5:5:1, 11:11:1) is relatively uncommon. Hence, in this study, we focus on the determination of aerodynamic parameters of rock-like debris with the shapes 1:1:1, 2:1:1, 2:2:1 and 3:1:1 shapes in this study, as all other shapes can be approximated as one of these.

1.6. Model algorithm

To account for the shape distribution found in the explosion of the ammunition magazine as well as for the factors identified earlier, we will now establish an algorithm that approximates the aerodynamic coefficients for each debris object.

We start by determining the shape drag of the debris object in the subsonic, incompressible regime. We distinguish here between low-aspect-ratio debris ($AR < 1.7$) and high-aspect-ratio debris ($AR > 1.7$). We refer to low-aspect-ratio debris from here on as sphere-like objects. Sphere-like objects will be treated with an interpolation between a sphere and a cube. Non-sphere-like objects are categorized according to their length ratios, and the aerodynamic coefficients are determined according to wind tunnel test data of similar objects.

Models to correct the drag coefficient for effects of the Mach number, cloud effect, debris roughness, and spin can be applied thereafter. However, the derivation of these corrections is not included in the scope of the present work.

2. Aerodynamic coefficients for sphere-like objects in subsonic conditions

We define all low-aspect-ratio fragments as sphere-like object, where $AR < 1.7$ as classified in section 1.6. For low-aspect-ratio debris, two extreme shapes can be identified: the sphere and the cuboid. Both can have quite different drag coefficients and, hence, a suitable interpolation between these extremes is needed. The volumes of these two extremes can be determined as:

- cuboid:

$$V_{\text{cuboid}} = L_{\max} \cdot L_2 \cdot L_3 \tag{10}$$

- ellipsoid:

$$V_{\text{ellipsoid}} = \frac{4}{3}\pi \cdot \frac{L_{\max}}{2} \cdot \frac{L_2}{2} \cdot \frac{L_3}{2} \tag{11}$$

Hence, we define the shape factor of the debris object as:

$$Sp = \frac{V_{\text{debris}} - V_{\text{cuboid}}}{V_{\text{ellipsoid}} - V_{\text{cuboid}}} \tag{12}$$

The shape factor Sp is unity if the fragment is a perfect sphere and zero if it is a perfect cube. We then define the drag of the sphere-like objects as:

$$C_{\text{D}} = Sp \cdot C_{\text{D,sphere}} + (1 - Sp) \cdot C_{\text{D,cube}} \tag{13}$$

The drag coefficient for a sphere has been frequently measured in the past. We use here the data collected by Schlichting [28] (Fig. 5). As the drag coefficient is dependent on the Reynolds number, this function would need to be parameterized. However, in practical applications for the speed of the debris found in the present application, the Reynolds number is

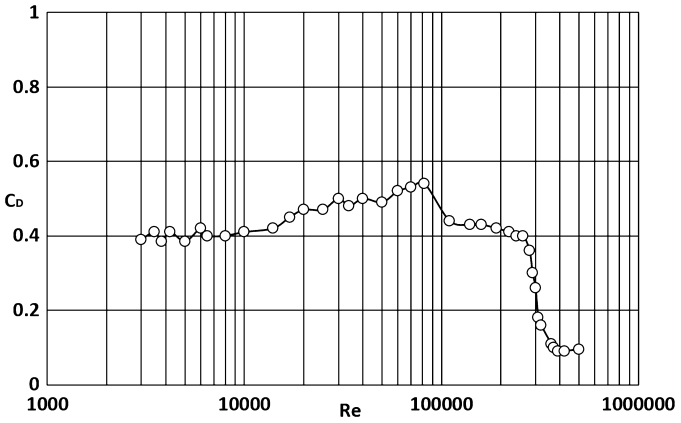

Fig. 5. Drag coefficient of a sphere in dependency on the Reynolds number.

generally in the range between $1{,}000 < Re < 200{,}000$ and the average drag coefficient $C_{D,\text{sphere}} = 0.42$ is a reasonable approximation. The average drag coefficient is determined based on the simulation database provided by Fan et al. [13], where an average Reynolds number of 190,000 is suggested for the initial break-up of the magazine. The drag coefficient $C_{D,\text{cube}}$ of the cube will be determined in wind tunnel tests in the following section.

Since the lift of spheres is zero, the lift coefficient reduces to:

$$C_L = (1 - Sp) \cdot C_{L,\text{cube}} \tag{14}$$

with $C_{L,\text{cube}}$ determined from the wind tunnel experiments in the next section.

3. Aerodynamic coefficients for cuboid objects in subsonic conditions

To determine the drag and lift coefficients for non-sphere-like objects, we have conducted a series of experiments in a wind tunnel to catalog frequently occurring classes of shapes classified by their length ratio. Length ratios 1:1:1, 2:1:1, 2:2:1, and 3:1:1 were studied. The debris objects were manufactured with plexiglass and the surface of the objects was polished (Fig. 6), indicating negligible friction drag. Perfect cuboid shape objects were used, i.e. with cuboid size of 50 mm (width) $\times$ 50 mm (height) $\times$ 50 mm (length) for the length ratio 1:1:1 case, for instance.

3.1. Experimental setup and procedures

Wind tunnel tests in subsonic condition were conducted in a closed loop wind tunnel from STEM ISU Impianti SpA at Nanyang Technological University to determine the aerodynamic coefficients (C_D and C_L). The size of the test section of this wind tunnel is 780 mm (width) $\times$ 720 mm (height) $\times$ 2000 mm (length). The speed range is 10–90 m/s and the turbulence level is about 0.1% as measured with a constant-temperature anemometer hotwire. The wind tunnel wall effect is considered to be insignificant where the solid blockage ratio falls well into the optimal wind tunnel operation range of 0.01–0.1 [29]. The wind tunnel background noise is not considered in the present setup, though background noise is found to be important in recent researches [30–32]. More literature on wind tunnel operation and measurement correction is available here [29,33,34]. Force measurements were taken with an internal balance mounted on a model positioning system (Fig. 6). With a special designed adaptor, the ranges of incidence angle (pitch angle) were allowed to be adjusted from 0 degree to 90 degrees. Calibration of the internal balance was conducted for lift and drag. The readings were taken for loads of up to 600 N. The manufacturer's accuracy was provided as 0.1% of the full load capacity of 2500 N and, hence, measurements were accurate within 2.5 N. Our calibration of the balance right before our measurements using static check loads surpassed the accuracy given by the manufacturer.

To assess whether the presence of the sting balance alters the drag coefficient of the model, we have performed CFD simulations with and without the sting, and no significant influence of the sting on the drag was identified.

3.2. Results: independence of the Reynolds number

First, we would like to demonstrate that the wind tunnel results obtained are independent of the Reynolds number within the scope of the present study. Fig. 7 shows the drag coefficient of a cuboid with an aspect ratio of 3:1:1 for different Reynolds number conditions. The variations of the drag coefficients at different Reynolds number conditions are relatively small in general, though deviations of drag coefficient values are identified with small incidence angles (5 degrees and 10 degrees). The relatively large deviation of the drag coefficient with small incidence angles is due to small projected area facing the flow (5 and 10 degree incidence angle) and thus the drag coefficient is more sensitive to the change of absolute

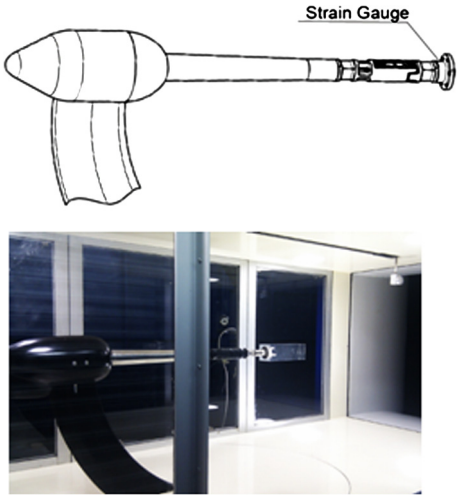

Fig. 6. Model positioning system with strain gauge internal balance (top), experimental setup (bottom).

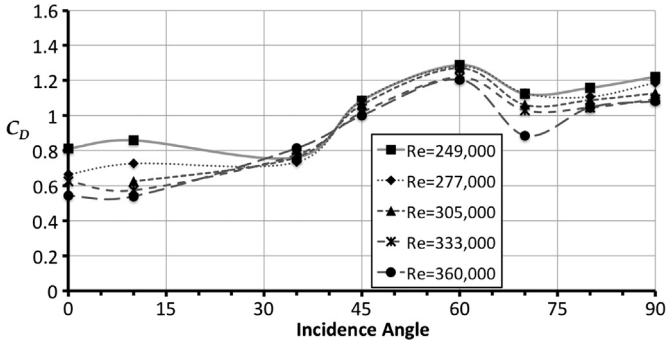

Fig. 7. Drag coefficient as function of incidence angle of a cuboid with an aspect ratio of 3:1:1 for different Reynolds numbers.

drag value and measurement uncertainties (refer to Eq. (2)). Based on the experimental results presented in Fig. 7, we can conclude that the drag coefficient is largely independent of the Reynolds number with exception for small-incidence-angle conditions. The following investigation will not include Reynolds number effect and a fixed Reynolds number will be used throughout the subsequent experiments.

3.3. Results: lift and drag of cuboids

Next, we determine the drag and lift coefficients for the four models at different angles of attack. The objects were swept from 0 to 90 degrees with 0 degree being aligned with the axis defining $L_{\max}$. Figs. 8 to 15 show the results for the different experiments. Note that the results obtained considering a negative incidence angle, presented in Figs. 8–15, were inferred from the symmetry of the positive incidence angle measurements. Error bars for each data point are provided, determined according to the accuracy of the internal balance used, which is described in section 3.1.

To facilitate the implementation of this data into a solver calculating the trajectory of the debris, we have created curve fittings for the experimental data. The curve fittings are in form of a Fourier series to take the natural geometric symmetry into account. The Fourier curve fitting method is adopted as it most appropriately describes the distributions of drag and lift coefficients with incidence angles, for different aspect ratio objects under the present experimental conditions. Nevertheless, it has to be noted that the curve-fitting approach is not necessarily accurate, as a compromise of prediction of a few data points, which are off the main curve-fitting range as shown in Figs. 8–15, has to be made to achieve an acceptable average approximation for the general trend.

The curve fittings for the lift and drag of the cuboids are then given by

- **cuboid 1:1:1**

$$C_{\mathrm{D}} = 0.7719 + 0.134\ \cos(4\alpha) \tag{15}$$

$$C_{\mathrm{L}} = -0.1413\ \sin(4\alpha) \tag{16}$$

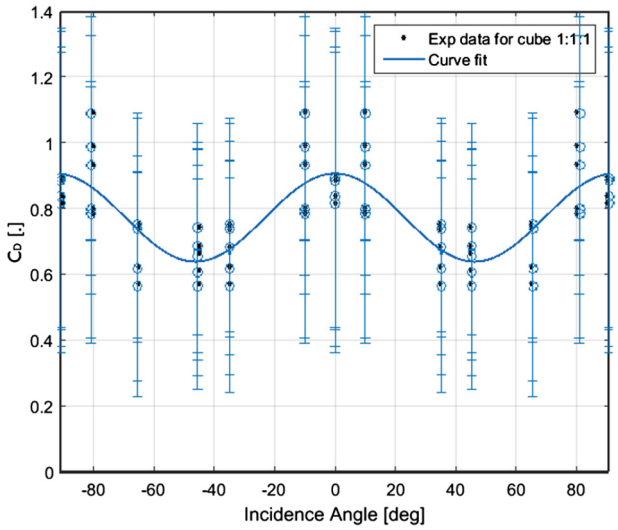

Fig. 8. Drag coefficients as a function of the incidence angle for a cuboid with an aspect ratio of 1:1:1.

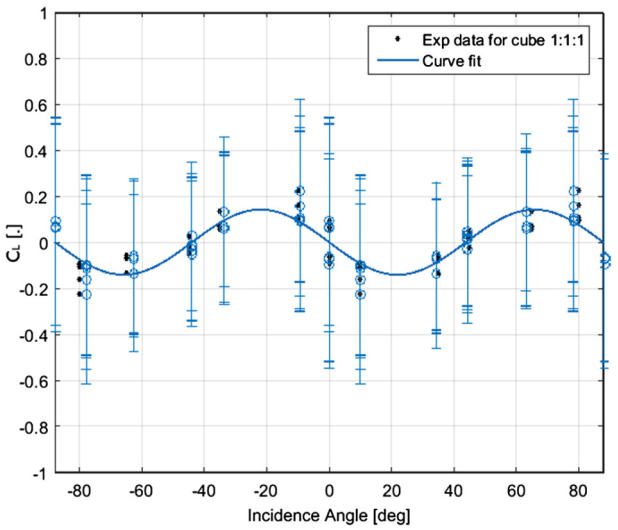

Fig. 9. Lift coefficients as a function of the incidence angle for a cuboid with an aspect ratio of 1:1:1.

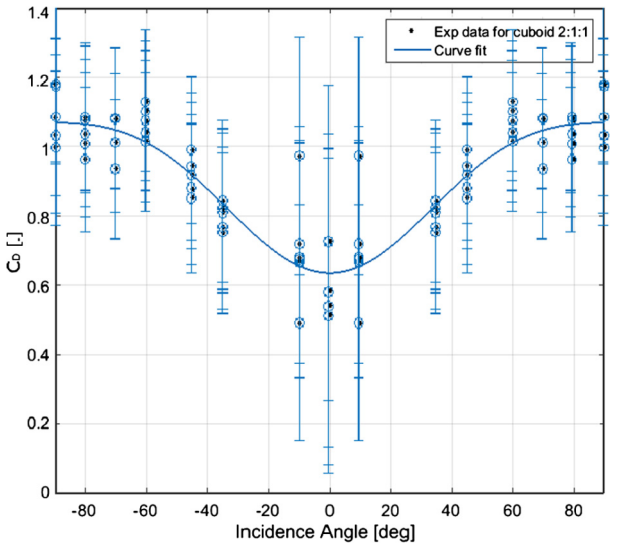

Fig. 10. Drag coefficients as a function of the incidence angle for a cuboid with an aspect ratio of 2:1:1.

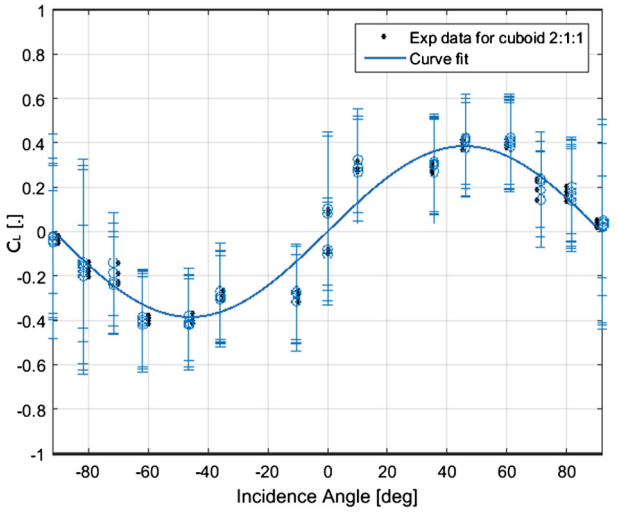

Fig. 11. Lift coefficients as a function of the incidence angle for a cuboid with an aspect ratio of 2:1:1.

- **cuboid 2:1:1**

$$C_D = 0.8604 - 0.2144\ \cos(2\alpha) \tag{17}$$

$$C_L = 0.3849\ \sin(2\alpha) \tag{18}$$

- **cuboid 3:1:1**

$$C_D = 0.8963 - 0.2601\ \cos(2\alpha) \tag{19}$$

$$C_L = 0.5768\ \sin(2\alpha) \tag{20}$$

- **cuboid 2:2:1**

$$C_D = 0.5855 + 0.08606\ \cos(8\alpha) \tag{21}$$

$$C_L = 0.5726\ \sin(2\alpha) \tag{22}$$

This database of drag and lift coefficients can be used for the computation of the trajectory of debris objects.

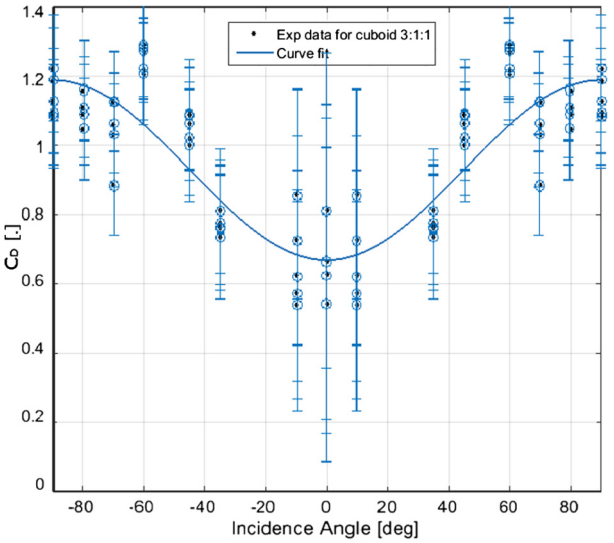

Fig. 12. Drag coefficients as a function of the incidence angle for a cuboid with an aspect ratio of 3:1:1.

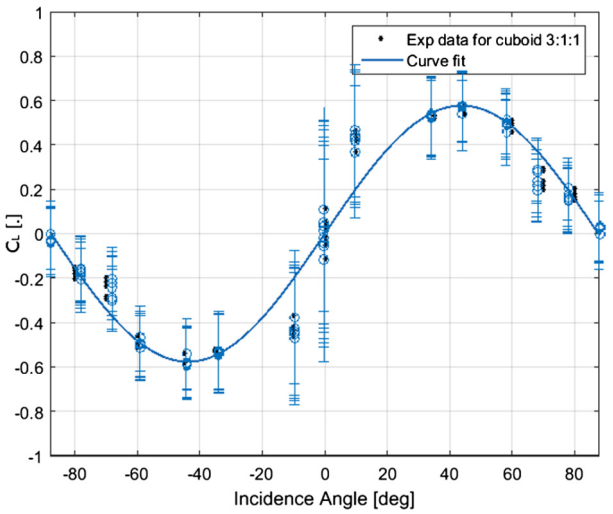

Fig. 13. Lift coefficients as a function of the incidence angle for a cuboid with an aspect ratio of 3:1:1.

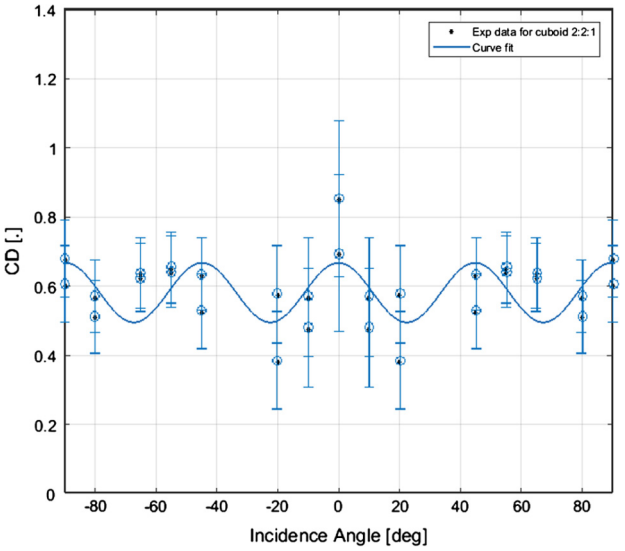

Fig. 14. Drag coefficients as a function of the incidence angle for a cuboid with an aspect ratio of 2:2:1.

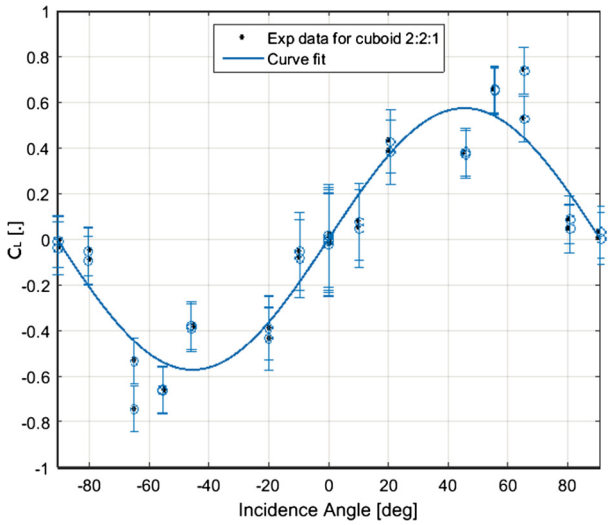

Fig. 15. Lift coefficients as a function of the incidence angle for a cuboid with an aspect ratio of 2:2:1.

4. Model validation

With the data available for the calculation of the debris, we would like now to validate and assess the accuracy of the model (Fig. 16). We have manufactured a total of 14 debris-like wind tunnel models. Three of these models were made out of concrete, while the remaining eleven were made out of Styrofoam (Fig. 17). Each model was tested at three different angles of attack ($\alpha = 0°,\ -10°,\ 20°$). We have then applied our proposed model and determined the difference between the model prediction and the actual wind tunnel measurements (Fig. 18). The tests were carried out at a wind speed of 50 m/s.

The drag coefficient C_D and the lift coefficient C_L obtained from the prediction model and the experiment are used to compute the total aerodynamic force coefficient C_F, which is given in the following general form:

$$C_F = \sqrt{C_D^2 + C_L^2} \tag{23}$$

The total aerodynamic force coefficient is calculated and presented along with the drag and lift coefficient in the following section, aiming to statistically show the correlations among these coefficient terms and determine the significance of each coefficient term for different tested objects. The results of the wind tunnel measurements are compared with the

Fig. 16. Example of concrete debris models.

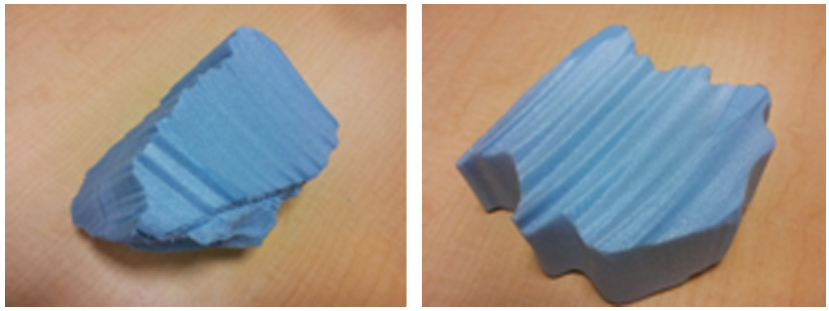

Fig. 17. Example of foam debris.

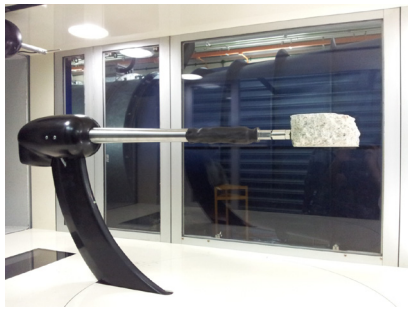

Fig. 18. Concrete debris model in the wind tunnel.

results of the prediction model, to show the performance of the proposed model in the prediction of drag, lift, and aerodynamic force coefficients. The tested objects are numbered according to their aspect ratio and testing incidence angle, such that objects from 1 to 20 represent results for cuboid-like debris (aspect ratio of 3:1:1, 2:1:1, and 2:2:1 respectively) and objects from 21 to 43 represent sphere-like debris (aspect ratio of 1:1:1). It is also pointed out from Figs. 19–24 for the cuboid-like data range and sphere-like data range respectively, to aid the understanding of the data presented. Fig. 19 shows the comparison of experimental measurement with the model prediction for the total aerodynamic force coefficient. The majority of both measured and predicted total aerodynamic force coefficients lies within the 0.4–0.8 range. Figs. 20 and 21 show the total drag force, drag component and lift component, respectively. The majority of the measured drag coefficients are again in the 0.4–0.8 range. The lift coefficients show large deviations in distribution compared to the drag coefficient. About 65% of measured lift coefficient lie within the −0.2–0.2 range, showing that lift plays a minor role in the total aerodynamic force, as its value is significantly less than measured or predicted drag.

The errors (in percentage) between experimental measurements and model predictions were calculated and are presented below. The error in the total aerodynamic force coefficient is defined as:

$$\Delta C_{\mathrm{F}} = \frac{C_{\mathrm{F,Model}} - C_{\mathrm{F,Exp}}}{C_{\mathrm{F,Exp}}} \cdot 100\% \tag{24}$$

The error in the total aerodynamic force due to the drag component is defined as:

$$\Delta C_{\mathrm{D}} = \frac{C_{\mathrm{D,Model}} - C_{\mathrm{D,Exp}}}{C_{\mathrm{F,Exp}}} \cdot 100\% \tag{25}$$

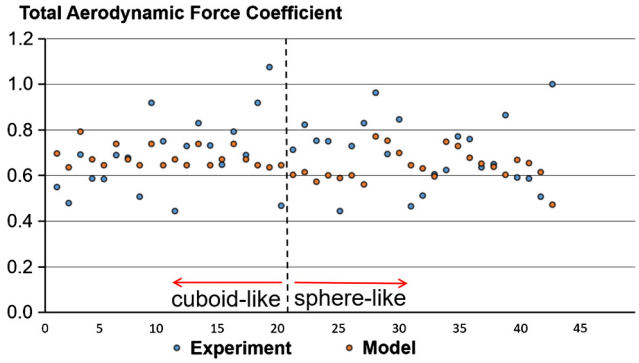

Fig. 19. Comparison of the values of the total aerodynamic force coefficient obtained from measurement and model prediction.

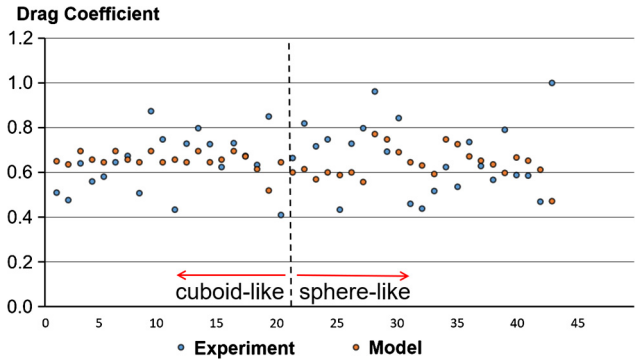

Fig. 20. Comparison of the values of the drag component obtained from measurement and model prediction.

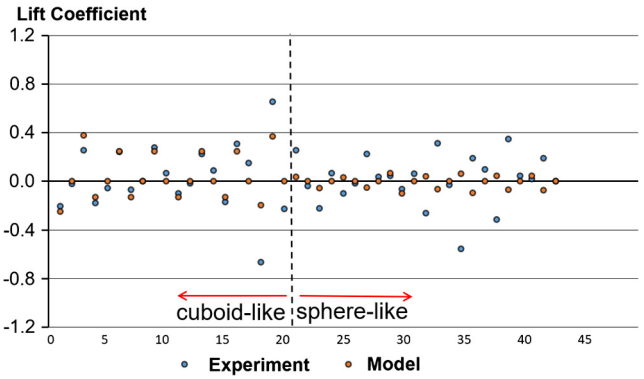

Fig. 21. Comparison of the values of the lift component obtained from measurement and model prediction.

The error in the total aerodynamic force due to the lift component is defined as:

$$\Delta C_L = \frac{C_{L,\mathrm{Model}} - C_{L,\mathrm{Exp}}}{C_{F,\mathrm{Exp}}} \cdot 100\% \tag{26}$$

The error in the total aerodynamic force coefficient is plotted in Fig. 22. We can identify a few debris objects where the error in prediction is large, some as high as 50%. However, for 74% of all measurement points, the predicted total aerodynamic force coefficient is within an error margin of ±25%. This can be considered a good agreement as the flow around the debris is very complex and yet the main aerodynamic force characteristics are predicted within this margin for the large majority of objects. Even more encouraging is the average error. Since the ammunition storage magazine explosion involves several thousand objects, an underestimation of the drag of one debris can be compensated by the overestimation of another one. The average error in total force is 0.6%, the median error is 1.6%, and the standard deviation is 23.3%.

A similar picture of error due to the drag component prediction is plotted in Fig. 23. As drag plays a critical role in the total aerodynamic force compared to the lift, the distribution of the drag error is very similar to that of the total aerodynamic force, and most debris objects are well within an error margin of ±25%. The average error in drag coefficient

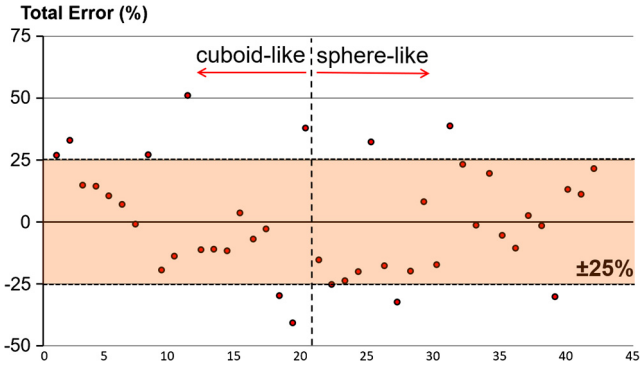

Fig. 22. Error in the total aerodynamic force coefficient between experimental measurement and model prediction. A majority of measurement points are within an error of ±25%.

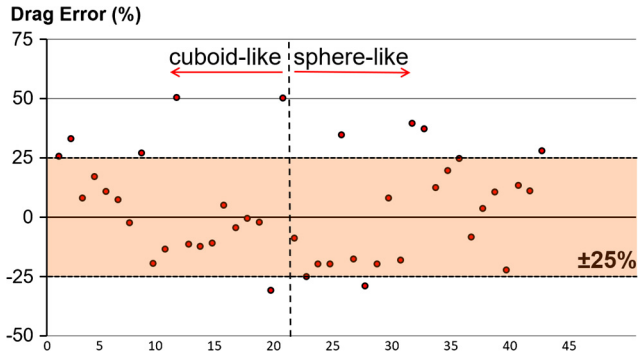

Fig. 23. Error in the experimental drag component between measurement and model prediction. A majority of measurement points are within an error of ±25%.

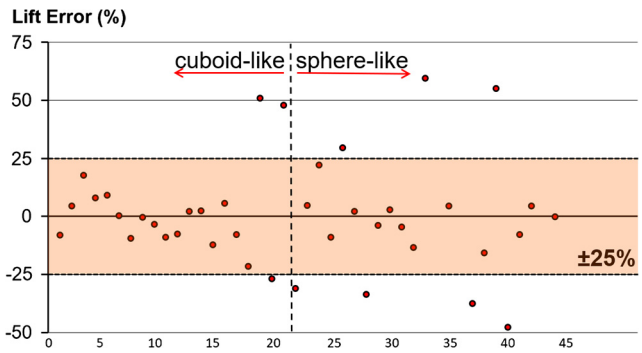

Fig. 24. Error in the experimental lift component between measurement and model prediction. A majority of measurement points are within an error of ±25%.

is 3%, the median error is 3.7%, and the standard deviation is 23.3%. Hence, the wind tunnel measurements of debris-like objects suggest that the model predicts the total aerodynamic force coefficient and drag coefficient reasonably well.

The errors due to the lift component prediction show a similar picture (Fig. 24). The error is generally smaller compared with the error in total force and drag, though some off-range points gave an error as high as 60%. However, for 56% of all measurement points, the predicted lift coefficient is within an error margin of 10%. For 77% of all measurement points, the predicted lift coefficient is still within an error margin of 25%. Considering the relative small value of lift compared with drag, this is reasonable, as the lift value will influence the total force to a small extent. In fact, we have determined from our wind tunnel results that the lift component magnitude is always less than 30% of the drag. The average error in lift prediction is 0.3%, the median error is 0.4%, and the standard deviation is 28.6%. Hence, even though deviation in lift prediction exists in some points, the model offers a reasonably good prediction of the majority of the lift values measured from the wind tunnel experiment.

Hence, we conclude that, while large errors may occur for individual debris, our model for the determination of the aerodynamic coefficients of rock-like debris is a good approximation for further studies on debris trajectories of rock-like objects, if the number of rock-like objects is sufficiently large to statistically average out the individual errors.

5. Summary and future work

In this study, we have created a model for the prediction of aerodynamic coefficients for debris trajectories. The effects of shape and orientation were classified and compared with a database of wind-tunnel results for similar objects.

The prediction of aerodynamic forces is generally difficult due to the fact that rock debris come in a large variety of shapes and, hence, the model certainly will have shortcomings in the prediction of each individual drag coefficient. In fact, our validation study shows relative errors in the prediction of the aerodynamic force of over 50% in some cases. However, for the majority of debris objects that we measure in the wind tunnel, the coefficients of total aerodynamic force, drag, and lift can be predicted within an accuracy of 25%. In terms of the average error and median error of the mass number of objects tested in this study, the model provides reasonably good predictions, where less than 3% in average error and less than 4% in median error are achieved for all aerodynamic components, respectively.

The model presented here provides a crucial refinement in the range prediction of airborne debris. Future work will apply this model to the simulation of the break-up of ammunition magazines and refine the model to account for compressibility effects at high subsonic speeds.

Acknowledgements

We thank the support of the Singapore Defense Science and Technology Agency (DSTA) for their support under the “Prediction of Explosion Hazards from Earth Covered Magazine” (PTRC-CEE/DSTA/2010.02) project.

References

[1] H.S. Lim, et al., A review: numerical modeling of the debris throw of reinforced concrete structures under internal explosion, in: 34th DOD Explosive Safety Seminar, Portland, OR, USA, 2010.
[2] F. Moghim, F.T. Xia, L. Caracoglia, Experimental analysis of a stochastic model for estimating wind-borne compact debris trajectory in turbulent winds, J. Fluids Struct. 54 (2015) 900–924.
[3] A.J. Vance, J.M. Buick, J. Livesey, Aerodynamics of a Rugby Ball, J. Appl. Mech. 79 (2) (2012) 021020.
[4] S. Chen, D. Zhao, Numerical study of non-reacting flowfields of a swirling trapped vortex ramjet combustor, Aerosp. Sci. Technol. 74 (2018) 81–92.
[5] X.Q. Zhang, P. Theissen, J.U. Schlüter, Towards simulation of flapping wings using immersed boundary method, Int. J. Numer. Methods Fluids 71 (4) (2013) 522–536.
[6] X. Wen, H. Tang, On hairpin vortices induced by circular synthetic jets in laminar and turbulent boundary layers, Comput. Fluids 95 (2014) 1–18.
[7] S. Chen, D. Zhao, Numerical study of guide vane effects on reacting flow characteristics in a trapped vortex combustor, Combust. Sci. Technol. 190 (2018) 2111–2133.
[8] G. Liu, et al., Numerical simulation of flow behavior of liquid and particles in liquid–solid risers with multi scale interfacial drag method, Adv. Powder Technol. 24 (2) (2013) 537–548.
[9] P.A. Cundall, O.D.L. Strack, A discrete numerical model for granular assemblies, Geotechnique 29 (1) (1979) 47–65.
[10] J. Xiang, J. Heng, T.H. New, A numerical parametric and optimization study of an industrial air-slide conveyor system, Powder Technology 315 (2017) 367–378.
[11] J. Xiang, T.H. New, Numerical investigations on a small-scale air-slide conveyor, J. Appl. Fluid Mech. 12 (1) (2019).
[12] H. Komossa, et al., Transversal bed motion in rotating drums using spherical particles: comparison of experiments with DEM simulations, Powder Technology 264 (Supplement C) (2014) 96–104.
[13] S.C. Fan, et al., Study of debris throw and dispersion after break-up of reinforced concrete structure under internal explosion, in: 34th DoD Explosive Safety Seminar, Portland, OR, USA, 2010.
[14] P.J. Richards, Dispersion of windborne debris, J. Wind Eng. Ind. Aerodyn. 104–106 (2012) 594–602.
[15] M. Held, Blast impulse at very near distance, Propellants Explos. Pyrotech. 33 (5) (2008) 353–359.
[16] J.A.B. Wills, B.E. Lee, T.A. Wyatt, A model of wind-borne debris damage, J. Wind Eng. Ind. Aerodyn. 90 (4–5) (2002) 555–565.
[17] M. Tachikawa, Trajectories of flat plates in uniform flow with application to wind-generated missiles, J. Wind Eng. Ind. Aerodyn. 14 (1–3) (1983) 443–453.
[18] J.D. Holmes, C.W. Letchford, N. Lin, Investigations of plate-type windborne debris – part II: computed trajectories, J. Wind Eng. Ind. Aerodyn. 94 (1) (2006) 21–39.
[19] J.D. Holmes, Trajectories of spheres in strong winds with application to wind-borne debris, J. Wind Eng. Ind. Aerodyn. 92 (2004) 9–22.
[20] C.J. Baker, The debris flight equations, J. Wind Eng. Ind. Aerodyn. 95 (5) (2007) 329–353.
[21] M. Grayson, W.C. Pang, S. Schiff, Three-dimensional probabilistic wind-borne debris trajectory model for building envelope impact risk assessment, J. Wind Eng. Ind. Aerodyn. 102 (2012) 22–35.
[22] A. Karimpour, N.B. Kaye, On the stochastic nature of compact debris flight, J. Wind Eng. Ind. Aerodyn. 100 (1) (2012) 77–90.
[23] E.M. Paul, TRAJ – A Two Dimensional Trajectory Program for Personal Computer, Defense Technical Information Center, Fort Belvoir, VA, USA, 1990.
[24] M.M.v.d Voort, R.J.M.v. A., Y.S. K., Ballistic Filtering for Improved Trajectory Calculations in the KG Software, TNO report, 2010, TNO-DV 2010 C071.
[25] G. Frank, Gouldstone, A.H. Craig, The UK structural debris throw model, in: 31st DOD Explosive Safety Seminar, San Antonio Marriott Rivercenter, 2004.
[26] R. Berglund, et al., Break up Tests with Small “Ammunition Houses”, Kasun II, FOI-R–2202-SE. Forsvarsbygg Report 51/06. Technical report, December 2006.
[27] C. Cusatis, et al., Towards the computational analysis of blast induced debris dynamics, in: International Symposium on Military Aspects of Blast and Shock (MABS21), 2010.
[28] H. Schlichting, Boundary-Layer Theory, 8th ed., Springer, 2000.
[29] X. Ji, Design and Analysis on Small Scale Fixed Pitch Straight Bladed Vertical Axis Wind Turbine (SB-VAWTs), PhD thesis, School of Mechanical and Aerospace Engineering, Nanyang Technological University, Singapore, 2012.

[30] R. Stoker, K. Ahuja, J. Hsu, Separation of wind-tunnel background noise and wind noise from automobile interior measurements, in: Proc. 2nd Aeroacoustics Conference, State College, PA, USA, American Institute of Aeronautics and Astronautics, 1996.
[31] X. Li, D. Zhao, X. Li, Effects of background noises on nonlinear dynamics of a modelled thermoacoustic combustor, J. Acoust. Soc. Am. 143 (1) (2018) 60–70.
[32] K. Pascioni, et al., Characterization of an aeroacoustic wind tunnel facility, in: inter.noise 2014, 43rd International Congress on Noise Control Engineering, Melbourne, November 16–19, 2014, Australian Acoustical Society, 2014, pp. 16–19.
[33] H.C. Garner, et al., Subsonic Wind Tunnel Wall Corrections, North Atlantic Treaty Organization, 1966.
[34] M.L. Laster, Wall Interference in Wind Tunnels, North Atlantic Treaty Organization, 1983.